INTL JOURNAL OF ELECTRONICS AND TELECOMMUNICATIONS, 2024, VOL. 70, NO. 4, PP. 879-886
Manuscript received May 16, 2024; revised October, 2024. doi: 10.24425/ijet.2024.152073

Bladder volume estimation based on USG images

Volodymyr Mosorov, Daniel Baradziej, Marta Chodyka

***Abstract*—The article explores deep learning models in urological diagnostics to measure urinary bladder volume from medical images. It addresses the shortcomings of traditional methods by introducing advanced imaging techniques for more objective and precise analysis. The research employs Convolutional Neural Networks (CNNs) and the MONAI platform for image segmentation and analysis, using data from The Cancer Imaging Archive to focus on urological regions. Findings suggest these models enhance diagnostic accuracy but also highlight the need for further modifications to tailor them to specific medical data, underscoring machine learning's significant role in accurate medical assessments for urology.**

***Keywords*—deep learning; bladder volume estimation; medical imaging convolutional neural networks; image segmentation; MONAI platform; diagnostic accuracy**

I. Introduction

THE fusion of medical imaging technology with advancements in artificial intelligence and machine learning has unveiled new opportunities in diagnostic and health condition monitoring domains. A notable application of these innovations is in urology, particularly in assessing the volume of the urinary bladder. Accurately knowing the bladder volume is crucial for diagnosing various urological conditions, including lower urinary tract disorders and other states affecting the bladder's capacity to efficiently store and evacuate urine. Traditional methods of bladder volume assessment often rely on techniques that might be invasive or imprecise, leading to a need for manual calculations and interpretations which carry risks of errors and subjectivity. Addressing these challenges, our study leverages advanced deep learning models to automate and enhance the precision of bladder volume measurement. This paper employs Convolutional Neural Networks (CNNs) to analyze medical images from The Cancer Imaging Archive [26], focusing on urinary system CT scans. The primary goal is not only to automate the volume measurement process but also to enhance its accuracy and repeatability through the application of deep learning models trained on extensive datasets. Using the Medical Open Network for AI (MONAI) platform, which provides tools specially tailored for medical image processing and analysis, bladder segmentation was performed. The efficacy of the models was evaluated using metrics such as the Dice similarity coefficient, allowing for detailed assessment of their precision and effectiveness in differentiating anatomical structures. It is expected that the findings will contribute to a better understanding of machine learning's applicability in practical medical diagnostics, offering a tool that could improve patient life quality through faster and more accurate diagnosis and monitoring of urological conditions.

II. Objectives

The urinary bladder, a key component of the urinary system, has an elastic structure that adapts to varying fluid volumes, playing a crucial role in the body's homeostasis. It is located in the extra peritoneal space of the pelvis behind the pubic bones and expands towards the abdominal cavity as it fills with urine. Bladder capacity is measured by analysing its ability to store fluids. There is no standard bladder size as it is an expansible organ, and its volume depends on various factors, including genetic and disease-related ones. Hence, assigning a specific average value for an individual without prior medical scan analysis is impractical. While the accepted average bladder capacity is around 500 ml, this value might be overly generalized. Individual differences in bladder capacity can stem from factors like gender, age, fluid consumption habits, anatomical conditions, and health status. Diseases such as diabetes, neurological issues, or urinary system infections can also alter its size. According to study [14], the normal bladder capacity in adults ranges between 300 to 400 ml. Different scenarios may occur in the elderly and children. For example, in the elderly, a decrease in bladder elasticity affects its capacity. In children aged 2-12 years, maximum bladder capacity can be calculated using the formula (1):

$$(\text{age} + 2) \times 30\text{ml} \tag{1}$$

Diagnostic images are used to measure the bladder's maximum depth, width, and height, which allows calculating an individual's bladder capacity. The standard computational formula with a correction factor of 0.75 as per [2] is presented as follows (2):

$$\text{width} \times \text{height} \times \text{depth} \times \text{correction factor} = \text{volume} \tag{2}$$

This method, according to research [4], generates a measurement error of about 8.57%.

Bladders can assume various shapes, adding complexity to the use of the formula. Identified bladder shapes include cuboid, ellipsoidal, trapezoidal, and elongated ellipsoidal. Different correction coefficients apply to these shapes: 0.89, 0.81, 0.66, and 0.52, respectively. Based on results [1], the standard correction coefficient for irregularly shaped bladders was estimated at 0.72. These coefficients have also been tested in studies [9], allowing adjustments to calculations to optimize values for various test scenarios and bladder shapes. The study also found that a coefficient of 0.72 provides the most accurate measurement results for many cases. In this work, the authors adopted the value of 0.72 as suitable and it will serve as a

First two Authors are with Lodz University of Technology, Poland (e-mail: volodymyr/mosorov@kis.p.lodz.pl).

Second Author is with John Paul II University in Biala Podlaska, Poland (e-mail: m.chodyka@akademiabialska.pl).

reference value for further assessments. Using MicroDicom software, bladder dimensions can be determined based on study results. An example bladder shown in Fig. 1 had dimensions of 5.71 mm x 3.75 mm x 4.53 mm. Using formula 1, the bladder volume was (3):

$$5.71\text{mm} \times 3.75\text{mm} \times 4.53\text{mm} \times 0.72 \approx 96.998\text{cm}^3 \approx 97\text{ml} \quad (3)$$

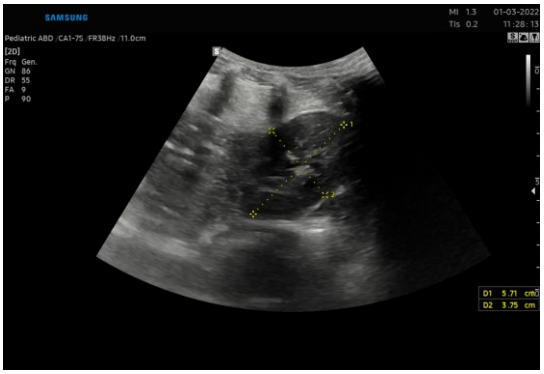

Fig. 1. Measurement of bladder dimensions

Accurate measurement of urinary bladder volume is crucial in urological diagnostics, monitoring bladder dysfunction, and assessing the effectiveness of treatment. Modern technologies such as advanced image analysis algorithms enable automatic detection and calculation of organ volumes. In radiological diagnostics, computed tomography (CT) imaging offers a detailed analysis of internal body structures, including the urinary bladder. Research authors [17] present the use of Convolutional Neural Networks (CNN) for automated kidney volume estimation based on low-dose unenhanced CT scans. Although the study focuses on kidneys, similar approaches can be applied for precise volume measurements of other organs, including the bladder. Techniques that allow in-depth image data analysis are crucial in precise diagnostics and monitoring of pathological states [6], [7], [11], [13]. In the processing, specialized tools such as MicroDicom, 3D Slicer, and OsiriX lite are used. These tools offer features from simple image manipulations to advanced visualizations and segmentations essential for accurate diagnostics. The choice of appropriate software depends on the specific needs of the user and the type of studies being performed [20]-[22]. These tools meet various medical needs from simple image manipulations to complex analyses and visualizations: MicroDicom is a free application for viewing medical images in DICOM or NifTi formats, allowing manipulation of photos (zooming, rotating, adjusting contrast and brightness) and saving them in various formats such as JPEG or PNG [27]. 3D Slicer is a free program for three-dimensional visualization that allows image editing on three planes and manual modelling of organs in 3D [28]. OsiriX lite offers features for viewing, manipulating, and analysing medical images, with an advanced paid version that enables 3D reconstructions and data management [29]. These tools support doctors in diagnostics, therapy planning, and disease monitoring, being useful mainly for medical specialists due to complex functionality. In response to the needs of inexperienced users, AI-based systems are being developed, enabling automatic segmentation and classification of medical images.

Image segmentation is a crucial step in preparing for computer-assisted surgeries, allowing precise planning of the procedure based on a three-dimensional model of the organ to be operated on [5], [10]. Such a 3D model, created through the segmentation process from a set of medical images, enables precise identification of areas that are the subject of surgical intervention. The segmentation process, which involves dividing the image into individual areas based on the similarity of neighboring pixels, is extremely important not only for feature extraction and measurements but also for improving the visibility of images during diagnostics [12], [15], [16], [19], [23]-[25]. In studies [8], [9], segmentation based on deep learning was applied using a convolutional neural network (CNN) optimized to operate on a system-on-chip (SoC). This network is adapted to work on devices with limited computing resources, using a multi-task architecture for simultaneous classification and segmentation of the image, which allows for effective differentiation of areas of interest from the background and for determining the volume of the bladder based on segmented images. Predefined similarity criteria based on pixel properties allow for efficient separation of individual anatomical elements, which is crucial in the process of disease detection and in Computer-Aided Diagnosis (CAD). CAD systems support doctors in interpreting radiological images, facilitating early detection of anomalies. They use image processing algorithms and techniques to improve the quality of scans, significantly contributing to the effectiveness of diagnostics. The analysis of principal components and the use of the Dice similarity measure, which is an indicator of the fit of segmentation to the actual area of interest, allows for the assessment of the precision of the segmentation process. The Dice measure, ranging between 0 and 1 where 1 indicates perfect matching, is fundamental for assessing the accuracy of organ or tissue segmentation, and values closer to 0 indicate poor fitting. This has a direct impact on the accuracy of the diagnosis and the effectiveness of treatment planning. In the case of the urinary system, precise segmentation is essential for assessing the condition of the kidneys and the urinary bladder. These techniques, using advanced image processing algorithms, allow for precise differentiation of individual anatomical structures, opening up new possibilities in diagnostic and interventional medicine.

Currently, many technologies allow for the visualization of individual parts of human anatomy that do not require the user to have specialized medical knowledge. A general understanding of programming languages and the principles of operation of models based on neural networks is sufficient. One such innovative solution is a set of models developed by the Medical Open Network for Artificial Intelligence (MONAI). It is an open-source framework based on PyTorch, designed specifically for deep learning in the field of medical imaging. By utilizing X-ray images, it enables accurate segmentation and identification of selected organs. MONAI focuses on creating advanced, comprehensive training processes tailored to the needs of medical imaging, offering tools and components optimized for this specific field. The main goal of MONAI is to accelerate research and collaboration in the field of medical imaging by providing domain-optimized implementations of deep learning algorithms and specialized tools tailored to the unique requirements of medical imaging tasks. The platform has been developed in collaboration with multiple institutions and

aims to accelerate research and facilitate clinical collaboration in the field of medical imaging. The main goal of MONAI is to stimulate innovation through the development of software that supports the advancement of digital medicine. As part of MONAI Model ZOO, a collection of medical imaging models has been made available in the MONAI Bundle format. This collection offers a range of deep learning models designed for medical image segmentation. Model ZOO in the context of MONAI refers to a set of ready-to-use, pre-trained artificial intelligence models that can be used in various applications in medical imaging. These models are continuously refined, and tools for abdominal organ segmentation are being developed to meet the requirements of increasingly complex and extensive projects. Thanks to the involvement of the MONAI community, numerous models focused on specific anatomical structures are being developed. In the study, the "Wholebody CT segmentation" model was used, which contains pre-trained models for three-dimensional segmentation of 104 human body organs using the SegResNet network. This network operates on the principle of encoder-decoder with deep supervision and is intended for semantic segmentation. Using this model requires downloading data and integrating it into a single NifTi file, with labels for each of the anatomical classes, ranging from soft tissues through the brain, organs, to bone structures. The model predicts the presence of 105 output channels, where the zero channel indicates the background, and the remaining 104 categories correspond to different foreground classes. The segmentation process of 104 tissue types is defined as multi-label segmentation, which requires a significant amount of GPU memory for correct calculation of indicators between the predicted mask and actual data. The requirements for hardware resources depend on the sizes of the input CT scan volume. The model was trained using a dataset used to create another deep learning model, TotalSegmentator, which automatically segments major anatomical structures in computed tomography scan images. The dataset utilizes 1,204 studies of various anatomical parts, including 27 organs, 59 types of bones, 10 types of muscles, and 8 vessels. Images were randomly drawn from routine clinical examinations, taking into account various age groups, tomographs, patient positions, and body parts. Two types of models are available, high and low resolution. The high-resolution model was trained on images where the pixel distance is 1.5 mm, while in the low-resolution model, the pixel spacing is 3 mm. The high-resolution model is characterized by greater accuracy, which, however, is associated with a greater demand for CPU resources and memory RAM needed to perform segmentation – over 26 GB compared to over 2 GB in the case of the low-resolution model. If the computer used to train the model has less RAM than required, the training process may significantly extend.

During the conducted research, the training process of the model was carried out using two hardware configurations. The first was a computer equipped with 16 GB of RAM and a quad-core processor with a clock speed of 3.4 GHz. The second computer had 8 GB of RAM and a processor with a clock speed of 4 GHz. Tests were conducted on a series of 152 image slices, which allowed for an examination of the time required to train the model depending on the available hardware resources. On the more advanced computer, the training time was 41 minutes, and the first results were obtained after just 3 minutes, while on the computer with less RAM, the process lasted 1 hour and 12 minutes, with the first results obtained after 7 minutes. In order to optimize time and resources, it was decided to focus research on the low-resolution model, using the high-resolution model only for comparative purposes.

For research purposes, X-ray images from The Cancer Imaging Archive [26], which were taken after the year 2000 and characterized by good resolution and quality, were selected, which was key for further analysis. 117 series of computed tomography images were selected to represent urological areas such as the bladder, pelvis, kidneys, prostate, and lower abdomen. Additionally, due to the need for high-quality data, studies performed after the year 2000 characterized by good resolution and image quality were chosen. The selected series contained between 70 to 300 images with clearly visible bladder structures.

As part of the conducted research, a set of advanced programming technologies and data processing tools were used, which enabled the development of a system for managing and analysing medical images. The technological basis of the project was the Python programming language in version 3.11.7, chosen for its versatility, extensive library supporting work with medical images, and a well-developed ecosystem of tools dedicated to machine learning. Work on the system was conducted in the Visual Studio Code programming environment, which offers support for various programming languages, including Python, providing a convenient and efficient environment for creating complex applications.

In the project, specialized libraries and tools supporting data processing and analysis as well as the design and training of machine learning models were used. Key technologies include: NumPy, PyTorch, PyDicom, Matplotlib, MONAI, Rt_utils, SciPy, IPython, and IPyWidgets. These tools enabled effective processing, analysis, and visualization of medical data, significantly expanding the possibilities for diagnostics, monitoring, and therapy of diseases, leveraging the latest achievements in the field of artificial intelligence and machine learning.

III. METHODS

The resolution of individual images varied depending on the visualization technique used, ranging from 512x512 to 1024x1024 pixels. Such diversity allowed for a wide spectrum of analysis in terms of image quality and detail in the context of the segmentation model's capabilities. To achieve optimal visualization and analysis of data, a series of transformations on selected computed tomography images was necessary. Examples of images from series 152 (Fig. 2) are photos with dimensions of 512x512 pixels, which corresponds to a size of 318 mm by 318 mm. Examples are shown based on images 110 and 120 in Fig. 2.

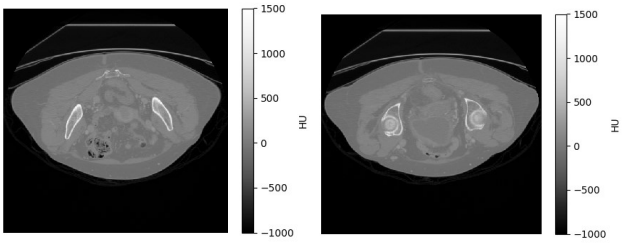

Fig. 2. Example images numbered 110 and 120 from series 152 of images

In Fig. 3, images from a series with dimensions of 512x512 pixels in a vertical projection with dimensions of 318 mm by 380 mm are presented. In this series, the size of a single section was 25 mm.

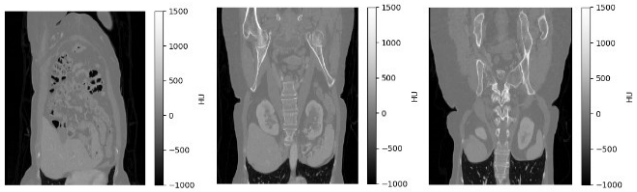

Fig. 3. Presentation of sections constructed based on computed tomography images

The use of the Hounsfield scale, a standard tool in CT image analysis, allows for accurate differentiation between different types of tissues based on their density. However, the challenge remained to adjust the contrast of images to ensure the visibility of anatomical details without losing significant information. The transformation of images to the "face-on" position utilized a rotation of 180 degrees around the newly defined Z-axis. This transformation aims to simulate a direct look at the examined body area, which is particularly important in the context of medical analysis where the orientation and position of anatomical structures play a key role. Assuming that the thickness of a single section is 25 mm, a technique was applied in which a series of images is viewed in reverse order. This way of presenting a series of images allows for more intuitive tracking of anatomical changes in cross-sections. Additionally, in the process of data analysis and presentation, tools for interactive viewing of sections were applied, as shown in Fig. 4.

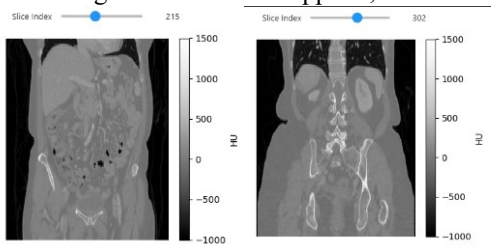

Fig. 4. Presentation of interactive section viewing

Thanks to this functionality, the user can carefully examine areas of interest, zoom in on them, and compare different sections. Interactive image viewing not only facilitates the detection of potential pathologies but also allows for a better understanding of complex anatomical structures.

An attempt was also made to optimize the contrast scale. Given the significant differences in X-ray absorption by air and bone tissue, represented respectively by values of -1000 and ≥1000 on the Hounsfield scale, adjusting the contrast scale became key. The goal was to achieve a level of contrast that would provide both sufficient differentiation between different types of tissues and the ability to clearly distinguish areas of similar density. Experiments with contrast adjustment aimed to find a balance that would not lead to excessive increase or decrease in differences, which could affect the difficulty of interpreting images. The application of advanced techniques for processing and analysing computed tomography images enables not only effective visualization of anatomical structures but also the introduction of methods for interactive data viewing. As a result, it is possible to better understand the dynamics of changes occurring in the examined urological areas, which is crucial in the diagnostic and therapeutic context.

IV. RESULTS

In the conducted research, this process was applied to process a series of X-ray images, resulting in two types of results, as presented in Fig. 5.

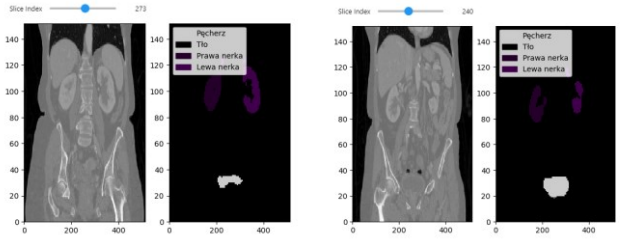

Fig. 5. Display of segmentation results next to the original image

The first result is the input image, which presents the state before segmentation. It allows for a general assessment of the condition of the examined area, but does not enable precise identification of structures within the urinary system without additional analysis. The second result, which is the effect of the segmentation process, presents the image after processing, where key organs of the urinary system are clearly marked. In the analysed example, structures such as the left and right kidney and the urinary bladder were identified and marked. Thanks to this method, it is possible to precisely isolate and visualize elements, which significantly facilitates further diagnostics and treatment planning. Further progress in the analysis of segmentation results allows for the use of the resulting mask generated by the segmentation model. The mask applied to the original image obtained from computed tomography allows for a visual assessment of the model's performance on individual image frames. This is crucial for assessing the precision and effectiveness of the applied model in the process of isolating specific anatomical areas, in this case, structures of the urinary system. This approach offers not only the possibility to verify which areas have been correctly identified and isolated by the model but also allows for noticing and analysing any imperfections or errors in segmentation. As a result, it is possible to make a more accurate assessment of the extent to which the model is reliable and whether it can be effectively used in practical medical diagnostics.

In Fig. 6, the result of segmentation on relevant sections performed by computed tomography is presented. The model mostly correctly segments organs, but does not mark their full shape. The model operates "conservatively," avoiding

unnecessary marking outside the area. This is important when, with the help of the performed segmentation, the program will create an approximate model of the patient's bladder.

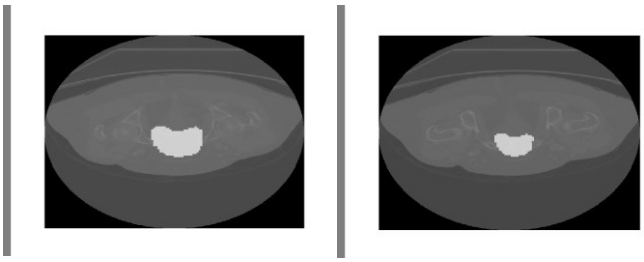

Fig. 6. Segmentation results superimposed on a computed tomography image

The study of bladder volume based on three-dimensional images is a key element in medical diagnostics, allowing for precise determination of its condition and function. In this process, advanced mathematical techniques such as analytic geometry and vector calculations were used, enabling accurate reconstruction and analysis of the 3D model. These techniques allowed for precise positioning of points relative to triangles defining the model surface, which was key for further calculations. After completing the image segmentation process, an analysis of the bladder volume was conducted. The result of the segmentation yielded a mask composed of voxels, i.e., three-dimensional cuboids, the sizes of which are specified in the study parameters. In this study, the height of one voxel was 25 mm, while its base is a square with a side length of 0.74 mm. These data enable the creation of a three-dimensional model compiled from individual sections (Fig. 7).

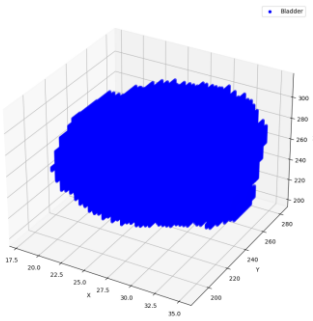

Fig. 7. Model generated based on segmentation

For accurate reconstruction of the model, triangulation techniques were used, which allowed for aggregating the volume occupied by the model. The presentation of the model after triangulation is shown in Fig. 8.

Based on the constructed bladder model, it was possible to accurately determine its volume. Using previously applied analytic geometry and vector calculations, an analysis of the position of points relative to triangles defining the model surface was conducted. This allowed for the aggregation of the volume occupied by the model, enabling a precise assessment of its dimensions.

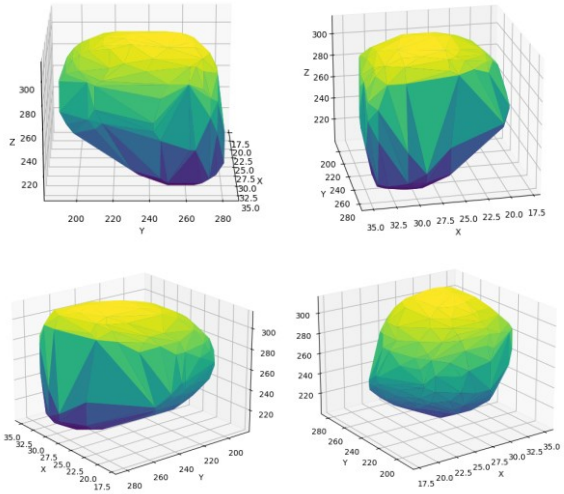

Fig. 8. Presentation of the model after triangulation

The volume of a single cell was calculated as the product of the dimensions of the cells in each dimension (4):

$$V_{cell} = d_x \cdot d_y \cdot d_z \tag{4}$$

where d_x, d_y, d_z st represent the dimensions of the cell along the x,y, z axes.

Subsequently, using vector calculations, the position of each point relative to the triangles $\overrightarrow{v0}, \overrightarrow{v1}, \overrightarrow{v2}$ (5) was defined:

$$\begin{aligned} \overrightarrow{v0} &= \overrightarrow{p2} - \overrightarrow{p0} \\ \overrightarrow{v1} &= \overrightarrow{p1} - \overrightarrow{p0} \\ \overrightarrow{v2} &= \vec{P} - \overrightarrow{p0} \end{aligned} \tag{5}$$

where $\vec{P}$ represents the vector point (x, y, z), and $\overrightarrow{p0}, \overrightarrow{p1}, \overrightarrow{p2}$ are the vectors of the triangle vertices.

In the next step, the vector product (6) and scalar product (7) were calculated to verify whether the vector $\vec{P}$ lies on the same side of the triangle.

$$\overrightarrow{v0} \times \overrightarrow{v1} \tag{6}$$

$$\left(\overrightarrow{v0} \times \overrightarrow{v1}\right) \cdot \overrightarrow{v2} \tag{7}$$

Calculations were repeated for each pair of vectors forming the edges of the triangle to ensure that the point is located inside all three half-planes defined by the triangle. The condition for placing the point inside the triangle was met when all scalar products took positive values.

In this study, the volume of the bladder amounted to 18,231 cm³. This result is smaller than the volume calculated manually by the authors, which amounted to 22,231.9 cm³. The difference in measurements was therefore 4,000.9 cm³.

In order to thoroughly examine the effectiveness and precision of the image segmentation program, tests were conducted on selected data sets from computed tomography scans. The tests aimed to assess the algorithm's ability to precisely segment anatomical structures under various conditions.

Set #2:

- Patient ID: TCGA-4Z-AA7Y
- Age of the subject: 60 years

- Distance between sections: 1.25 mm.
- Dimensions of a single scan in the series: 512 x 512 pixels
- Number of sections in the series: 423

In Fig. 9, sections and segmentations for set #2 performed by the lower-resolution model are presented:

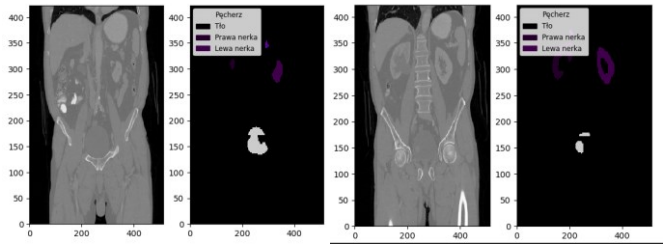

Fig. 9. Sections and segmentations for the second set, model of lower resolution

In the segmentation results, inaccuracy was noticeable, indicating that part of the bladder was not included. This could result from a very small distance between sections of 1.25 mm. Using a model trained on data with a slightly larger distance between sections, i.e., 1.5 mm, the segmentation results, as shown in Fig. 10, were significantly better.

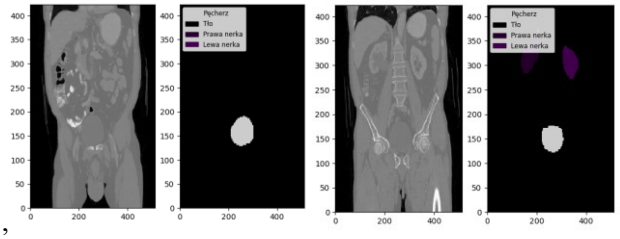

,

Fig. 10. Sections and segmentation for the second set, high-resolution model

The bladder volume for the patient from set #2 of data was 371.40 cm³ for the low-resolution model and 930.59 cm³ for the high-resolution model. The difference resulted from training sets adjusted to different quality images. In this case, matching under a specific type of study increased the result of the examined organ by 559.19 cm³. To confront the results, the size of the bladder was manually calculated using the previously given formula (Fig. 11).

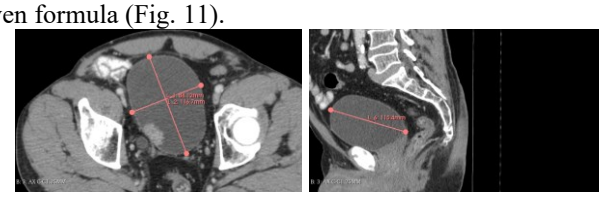

Fig. 11. Measurement of bladder sizes for set #2

According to calculations, the bladder volume for this patient is equal (8):

$$8412\text{mm}\times1167\text{mm}\times1154\text{mm}\times0.72=815.66\text{cm}^3 \quad (8)$$

Compared to calculations performed based on the created three-dimensional model, the difference amounted to 115.09 cm³, giving an area larger by about 14%.

Set #3:

- Patient ID: TCGA-ZF-AA5P
- Age of the subject: not available
- Distance between sections: 1.25 mm.
- Dimensions of a single scan in the series: 512 x 512 pixels
- Number of sections in the series: 235

Using a high-resolution model in the case of set #3 allowed for correct segmentation of urinary system organs. The bladder is clearly visible along with the kidneys (Fig. 12). According to the calculations obtained, the model volume amounted to 705.41 cm³.

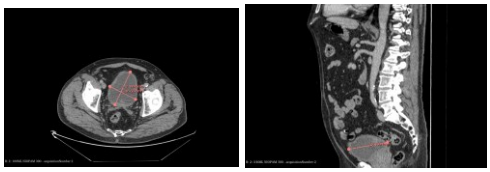

Fig. 12. Measurement of bladder sizes for the third set

Set #4:

- Patient ID: Pediatric-CT-SEG-00DCF4D6
- Age of the subject: 10 years
- Distance between sections: 2 mm.
- Dimensions of a single scan in the series: 512 x 512 pixels
- Number of sections in the series: 207

Fig. 13 presents segmentations for set #4 performed by the model of low and high resolution

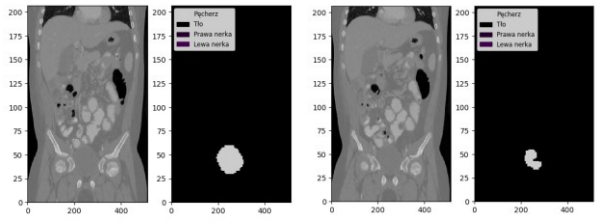

Fig. 13. Sections and segmentations for set #4, model of low resolution (on the left) and model of high resolution (on the right)

The bladder volume estimated using the low-resolution model amounted to 33,808 cm³, and for the high-resolution model, only 9,084 cm³, indicating significant issues related to the too large distance between sections, i.e., 2mm. This gap is 0.5 mm larger than that used in the training data. The structure formed by segmentation of the second model has missing outer shell elements. The shape of the obtained bladder is irregular and has a small volume. The organ was not segmented correctly, which reduced the final result of the calculations. The bladder volume for set #4, calculated based on Fig. 14, amounts to 23,728 cm³. It is 1,008 cm³ smaller and 14,644 cm³ larger than the results of the models.

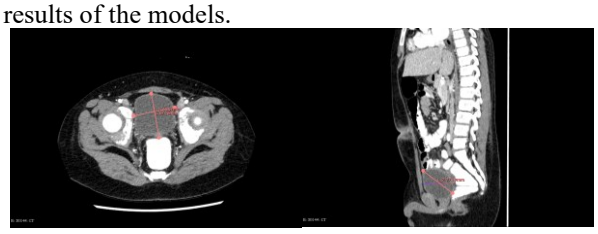

Fig. 14. Measurement of bladder sizes for the fourth set

In the tables below, a comparison of own calculations and computational results of models on available medical datasets is presented.

TABLE I
RESULTS OF BLADDER VOLUME STUDY FOR IMAGES WITH DIMENSIONS OF 512 X 512 PIXELS

	Calculated bladder volume		
Test set 512x512px (distance between sections)	Model of low resolution [cm³]	Model of high resolution [cm³]	Own calculations [cm³]
Set #5 (2 mm)	715,88	788,50	654,20
Set #6 (1,25 mm)	no segmentation	73,90	129,43
Set #7 (2,5 mm)	317,73	472,74	503,59

TABLE II
RESULTS OF CALCULATED BLADDER VOLUME FOR IMAGES WITH DIMENSIONS OF 1024 X 1024 PIXELS

	Calculated bladder volume		
Test set 1024x1024px (distance between sections)	Model of low resolution [cm³]	Model of high resolution [cm³]	Own calculations [cm³]
Set #8 (2 mm)	886,99	3112,43	345,00

During the analysis of the results, own methods should be considered, taking into account the lack of experience in analysing medical results. The calculations that have been made are highly approximate and may not reflect the results that could be obtained by a specialist in this field. However, based on the obtained results, it can be assumed that the model, appropriately adjusted to the input data, fulfills its segmentation task of urinary system organs.

During the research, challenges related to the diversity and quality of data, such as the heterogeneity of image resolution and differences in distances between sections, were encountered. The use of models with different resolutions allowed for the optimization of the segmentation and analysis process, adequately adjusting tools to the specificity of the data. It was also key to adjust the Hounsfield scale and image contrast to ensure the best readability and accuracy of the results. For research purposes, a set of eight series of urological examinations was singled out, covering patients aged from 10 to 60 years, both women and men. The collected data had different pixel distance parameters, affecting the overall resolution of the resulting image, with a range from 1.25 to 4 millimetres of distance between sections and a resolution from 512x512 pixels to 1024x1024 pixels.

DICOM format metadata from the saved computed tomography scans allowed for the display and processing of images created during the radiological procedure. These images were then segmented, allowing for the isolation of major organs of the urinary system. The applied models successfully segmented the study images. The three-dimensional bladder model created based on them was used to calculate its volume. The obtained results were compared with the results calculated based on existing images using 3D Slicer software. The difference between the best calculation for a given section and own calculations averaged approximately 923 cm³, which is a satisfactory result.

Models of different resolutions showed varied effectiveness in segmenting the urinary bladder, which was also evident in the analysis of volume. The high-resolution model for set #8 (size 1024x1024 pixels, distance between sections 2 mm) estimated the volume at 311,243 cm³, which significantly deviated from own calculations of 34,500 cm³. One of the main challenges was the heterogeneity and quality of data, which affected the effectiveness of the models. Some images were characterized by an irregular bladder shape and small volume, making precise segmentation difficult. Additionally, differences in distances between sections relative to the training data of the models could affect the results. For example, in the case of set #4 with a distance between sections of 2 mm, the high-resolution model recorded a significantly smaller volume (9,084 cm³) compared to the low-resolution model (33,808 cm³), suggesting that the model may not have been optimally adjusted to the analysed data. The research findings underline the potential of deep learning models for segmenting medical images, although they also indicate the need for further adjustment of models to the specifics of medical data. Effective segmentation and precise analysis of bladder volume can significantly support urological diagnostics, enabling better monitoring and planning of treatment.

CONCLUSION

This article presents the application of deep learning models for analysing the volume of the urinary bladder in medical images. The conducted studies showed that modern medical imaging technologies and advanced image analysis algorithms can significantly contribute to progress in urological diagnostics. Automatic segmentation of organs from DICOM images using machine learning algorithms opens up new possibilities in diagnostics, enabling quick and accurate analysis without the need for deep specialist knowledge. As a result, medicine becomes more accessible and effective, which is crucial in the rapid recognition and monitoring of many diseases.

The analysis of bladder volume conducted using deep learning models revealed differences between model calculations and manual volume calculations. Despite these differences, the segmentation models showed promising results in identifying key organs of the urinary system. However, in some cases, the models operated in a "conservative" manner, avoiding unnecessary marking outside the area of interest, which resulted in imperfections in fully replicating the shapes of organs. The use of deep learning models in medical image analysis offers new perspectives in precise urological diagnostics. Thanks to automatic organ segmentation, quick and accurate analysis is possible without the need for deep specialist knowledge, making medicine more accessible and effective. Nonetheless, the research results underscore the need for further development and adjustment of models to the specific requirements of medical data to increase their accuracy and clinical utility.

Future research should focus on developing more flexible models capable of adapting to the diversity of medical data and

on experiments with a larger amount of data. Moreover, it will be important to seek new methods and technologies that will better cope with challenges related to the diversity and quality of medical images. In summary, the use of deep learning models for analysing the volume of the urinary bladder in medical images represents an important step towards improving urological diagnostics. Further development of these technologies may bring significant benefits to medicine, offering tools that support doctors in accurate diagnostics, treatment planning, and monitoring disease progress.

REFERENCES

[1] Bih, L., Ho, C., Tsai, S., Lai, Y. i Chow, W., "Bladder shape impact on the accuracy of ultrasonic estimation of bladder volume", Archives of Physical Medicine and Rehabilitation, vol. 79, no.12, pp. 1553–1556, 1998. https://doi.org/10.1016/S0003-9993(98)90419-1

[2] Birch, N., Hurst, G., Doyle, P., "Serial Residual Volumes in Men with Prostatic Hypertrophy", British Journal of Urology, vol. 62, no. 6, pp. 571–575, 1988. https://doi.org/10.1111/j.1464-410X.1988.tb04428.x

[3] Bolla, S., Odeluga, N., Amraei, R., „Histology, Bladder" in StatPearsl [Internet]. Treasure Island (FL): StatPearls Publishing, 2024 Jan. Availavle online: https://www.ncbi.nlm.nih.gov/books/NBK540963/

[4] Chan, H. "Noninvasive bladder volume measurement". Journal of Neuroscience Nursing, vol. 25, no. 5, pp. 309-312, 1993. https://doi.org/10.1097/01376517-199310000-00007

[5] Christ, P.F., Elshaer, M.E.A., Ettlinger, F., Tatavarty, S., Bickel, M., Bilic, P., Rempfler, M., Armbruster, M., Hofmann, F., D'Anastasi, M., Sommer, W.H., Ahmadi, S.-A., Menze, B.H. "Automatic Liver and Lesion Segmentation in CT Using Cascaded Fully Convolutional Neural Networks and 3D Conditional Random Fields", Proceedings of the MICCAI, pp. 415-423, 2016. https://doi.org/10.48550/arXiv.1610.02177

[6] Esteva, A., Kuprel, B., Novoa, R.A., Ko, J., Swetter, S.M., Blau, H.M., Thrun, S. "Dermatologist-level classification of skin cancer with deep neural networks", Nature, vol. 542, pp. 115-118, 2017. http://doi.org/10.1038/nature21056

[7] Gibson, E., Li, W., Sudre, C., Fidon, L., Shakir, D.I., Wang, G., Eaton-Rosen, Z., Gray, R., Doel, T., Hu, Y., Whyntie, T., Nachev, P., Modat, M., Barratt, D.C., Ourselin, S., Cardoso, M.J., Vercauteren, T. "NiftyNet: A Deep-Learning Platform for Medical Imaging", Computer Methods and Programs in Biomedicine, vol. 158, pp. 113-122, 2018. https://doi.org/10.1016/j.cmpb.2018.01.025

[8] Han, X. "Automatic Liver Lesion Segmentation Using A Deep Convolutional Neural Network Method", arXiv preprint arXiv:1704.07239, 2018. https://doi.org/10.48550/arXiv.1704.07239

[9] Hyunwoo, C., Ilseob, S., Jihun, J.,Yangmo, Y., "A Lightweight Deep Learning Network on a System-on-Chip for Wearable Ultrasound Bladder Volume Measurement Systems: Preliminary Study", Bioengineering, vol. 10, no. 5, article number 525, 2023. https://doi.org/10.3390/bioengineering10050525

[10] Kamnitsas, K., Ledig, C., Newcombe, V.F.J., Simpson, J.P., Kane, A.D., Menon, D.K., Rueckert, D., Glocker, B. "Efficient Multi-Scale 3D CNN with Fully Connected CRF for Accurate Brain Lesion Segmentation", Medical Image Analysis, vol. 36, pp. 61-78, 2017. https://doi.org/10.1016/j.media.2016.10.004

[11] Kumar, A., Kim, J., Lyndon, D., Fulham, M., Feng, D. "An Ensemble of Fine-Tuned Convolutional Neural Networks for Medical Image Classification", IEEE Journal of Biomedical and Health Informatics, vol. 23, no. 1, pp. 314-323., 2019. https://doi.org/10.1109/JBHI.2016.2635663

[12] Li, X., Chen, H., Qi, X., Dou, Q., Fu, C.W., Heng, P.A. "H-DenseUNet: Hybrid Densely Connected UNet for Liver and Liver Tumor Segmentation from CT Volumes", IEEE Transactions on Medical Imaging, vol. 39, no. 6, pp. 1306-1317, 2020. https://doi.org/10.48550/arXiv.1709.07330

[13] Litjens, G., Kooi, T., Bejnordi, B.E., Setio, A.A.A., Ciompi, F., Ghafoorian, M., van der Laak, J.A.W.M., van Ginneken, B., Sánchez, C.I. "A survey on deep learning in medical image analysis', Medical Image Analysis, vol. 42, pp. 60-88, 2017. https://doi.org/10.1016/j.media.2017.07.005

[14] Lukacz, E., Sampselle, C., Gray, M., Macdiarmid, S., Rosenberg, M., Ellsworth, P., Palmer, M., "A healthy bladder: a consensus statement". International Journal of Clinical Practice, vol. 65, no. 10, pp. 1026-1036, 2011. https://doi.org/10.1111/j.1742-1241.2011.02763.x

[15] Memon, N., Mirza, A., Gilani, S., " Segmentation of Lungs from CT Scan Images for Early Diagnosis of Lung Cancer". World Academy of Science, Engineering and Technology. International Journal of Medical and Health Sciences, vol. 2, no. 2, pp. 297-302, 2008. Available online: https://api.semanticscholar.org/CorpusID:15484020

[16] Milletari, F., Navab, N., Ahmadi, S.-A., "V-Net: Fully Convolutional Neural Networks for Volumetric Medical Image Segmentation", Fourth International Conference on 3D Vision (3DV), pp. 565-571. 2016. https://doi.org/10.1109/3DV.2016.79

[17] Müller, L., Tibyampansha, D., Mildenberger, P., Panholzer, T., Jungmann, F., Halfmann, M.C., "Convolutional neural network-based kidney volume estimation from low-dose unenhanced computed tomography scans", BMC Medical Imaging, vol. 23, no. 1, article number 187, 2023. https://doi.org/10.1186/s12880-023-01142-y

[18] Mustra, M., Delac, K., Grgic., M., "Overview of the DICOM standard" in 2008 50th International Symposium ELMAR, Borik Zadar, Croatia: IEEE, pp. 39-44, 2008. Available online: https://ieeexplore.ieee.org/document/4747434

[19] Ronneberger, O., Fischer, P., Brox, T., "U-Net: Convolutional Networks for Biomedical Image Segmentation", Medical Image Computing and Computer-Assisted Intervention – MICCAI 2015 Eds. Navab N., Hornegger J., Wells W., Frangi A. Cham; Springer, pp. 234-241, 2015. https://doi.org/10.1007/978-3-319-24574-4_28

[20] Rosenberger, R., Wojtek, P., Konopka, M., Pieniążek, P., Bogusz, I., Sąsiadek, M., „Kliniczne zastosowanie obrazowania perfuzyjnego metodą tomografii komputerowej oraz obrazowania dyfuzyjnego i perfuzyjnego metodą rezonansu magnetycznego w wykrywaniu wczesnych zmian w udarze niedokrwiennym mózgu", Udar Mózgu. Problemy Interdyscyplinarne, tom 6, no 2, pp. 71–78, 2004. Available online: https://journals.viamedica.pl/um/article/view/33754/24796

[21] Setio, A.A.A., Traverso, A., de Bel, T., Berens, M.S.N., van den Bogaard, C., Cerello, P., Chen, H., Dou, Q., Fantacci, M.E., Geurts, B., van der Gugten, R., Heng, P.A., Jansen, B., de Kaste, M.M.J., Kotov, V., Lin, J.Y.-H., Manders, J.T.M.C., Sánchez, C.I., Schaap, M., Silva, C.A., Snoeren, M., Prokop, M., Smitsmans, M.H.P., Tang, H., Terraz, O., van Velden, F.H.P., Walsh, S., Zuidhof, G.C.A., van Ginneken, B., Jacobs, C., "Validation, Comparison, and Combination of Algorithms for Automatic Detection of Pulmonary Nodules in Computed Tomography Images: The LUNA16 Challenge", Medical Image Analysis, vol. 42, pp. 1-13, 2017. https://doi.org/10.1016/j.media.2017.06.015

[22] Shen, D., Wu, G., Suk, H.-I. "Deep Learning in Medical Image Analysis", Annual Review of Biomedical Engineering, vol. 19, pp. 221-248, 2017. https://doi.org/10.1007/978-3-030-33128-3_1

[23] Simpson, A.L., Antonelli, M., Bakas, S., Bilello, M., Farahani, K., van Ginneken, B., Kopp-Schneider, A., Landman, B.A., Litjens, G., Menze, B., Ronneberger, O., Summers, R.M., Bilic, P., Christ, P.F., Do, R.K.G., Gollub, M., Golia-Pernicka, J., Heckers, S.H., Jarnagin, W.R., McHugo, M.K., Napel, S., Vorontsov, E., Maier-Hein, L., Cardoso, M.J., "A large annotated medical image dataset for the development and evaluation of segmentation algorithms", arXiv preprint, 2019. https://doi.org/10.48550/arXiv.1902.09063

[24] Wasserthal, J., Breit, H.-C., Meyer, M. T., Pradella, M., Hinck, D., Sauter, A. W., Segeroth, M., "TotalSegmentator: Robust Segmentation of 104 Anatomic Structures in CT Images", Radiology Artificial Intelligence, vol. 5, no. 5, article number 230024, 2023. https://doi.org/10.1148/ryai.230024

[25] Zhou, Z., Rahman Siddiquee, M., Tajbakhsh, N., Liang, J., "UNet++: A Nested U-Net Architecture for Medical Image Segmentation" in Deep Learning in Medical Image Analysis and Multimodal Learning for Clinical Decision Support, vol. 11045, pp. 3-11, 2018. https://doi.opi/10.1007/978-3-030-00889-5_1

[26] Cancer Imaging Archive, https://public.cancerimagingarchive.net/, 2024.

[27] MicroDicom, https://www.microdicom.com/, 2024.

[28] 3D Slicer, https://www.slicer.org/, 2024.

[29] OsiriX Foundation, https://www.osirix-viewer.com/, 2024.